Asian Journal of Chemistry; Vol. 38, No. 6 (2026), 1482-1492
ASIAN JOURNAL OF CHEMISTRY
https://doi.org/10.14233/ajchem.2026.35830

Multifunctional Isoniazid-Derived Schiff Base Metal(II) Complexes: Synthesis, Characterization, Molecular Docking, DFT and Biological Studies

D.A. JENIVA and KANNAPAN GEETHA*,

P.G. and Research Department of Chemistry, Muthurangam Government Arts College, Otteri, Vellore-632002, India

*Corresponding author: E-mail: geethakg0503@gmail.com

Received: 27 February 2026 *Accepted*: 23 April 2026 *Published online*: 31 May 2026 AJC-22374

A series of novel transition metal complexes of Co(II), Ni(II), Cu(II), and Zn(II) derived from an isoniazid-based Schiff base ligand were synthesised and characterised using spectroscopic and analytical techniques including FT-IR, UV-visible, ESI-MS, elemental analysis, conductivity measurements and NMR spectroscopy. Spectral investigations confirmed the coordination of the ligand to metal ions through azomethine nitrogen and oxygen donor atoms, leading to stable non-electrolytic metal(II) complexes. The biological potential of the synthesised ligand and its metal(II) complexes was evaluated through antidiabetic, anti-inflammatory and antioxidant assays. All metal(II) complexes exhibited enhanced biological activity compared with the free ligand. Among the investigated complexes, Zn(II) complex demonstrated the highest anti-inflammatory activity (98.0%), while the Ni(II) complex showed superior antidiabetic activity with 96.2% α-amylase inhibition. The Cu(II) complex exhibited the strongest antioxidant activity (96.7%). The improved biological performance of the metal complexes is attributed to increased ligand–biomolecule interactions upon metal coordination. Molecular docking studies against the 1HNY protein revealed strong binding affinities of the complexes, particularly for the Zn(II) complex, which exhibited the highest binding energy (-271.76 kJ/mol) and multiple hydrogen-bonding interactions with amino acid residues. Density functional theory (DFT) calculations further supported the experimental findings by providing insights into electronic distribution, HOMO–LUMO energy gaps, molecular stability, electrophilicity and charge transfer behaviour. Molecular electrostatic potential (MEP) analysis confirmed the presence of active electrophilic and nucleophilic sites responsible for biomolecular interactions.

Keywords: Transition metal complexes, Biological activities, Molecular docking, DFT studies.

INTRODUCTION

The importance of small molecules in therapeutic drug development has increased significantly in recent years. Extensive research efforts are currently focused on the discovery and development of biologically active compounds with antimicrobial, antidiabetic, anti-inflammatory, antibacterial and antioxidant properties for potential biomedical and pharmaceutical applications [1]. The imine base containing small molecules shows higher activity in the treatment of bacterial and fungal infections. These types of drugs can be replaced by existing antimicrobial drugs [2-8]. Metformin and furazolidone deliver the good therapeutic nature of antidiabetics and antibacterials. Especially, benzoyl hydrazine shows a wide range of biological activities including antileishmanial [9], anti-inflammatory [10], anticancer [11], antimicrobial [12], properties, *etc*.

While carbon-containing small molecules exhibit significant drug activities, but most of these molecules produce higher side effects which reduces their utilisation [13]. Metal-based, especially first-row transition metals, offer enhanced bioactive nature and low side effects on human being. The chelation determined the number of bonds between metal and ligand (organic or inorganic molecules). It may be combined with one or more ligands with metal through coordination covalent bond [14].

Ligands act as secondary valence components in metal complexes and play a key role in determining the coordination environment and geometries around the metal center including tetrahedral, square planar, trigonal bipyramidal and octahedral structures. Unlike simple organic molecules, whose geometries are limited by the tetravalency of carbon, metal complexes exhibit greater structural diversity and tunable physicochemical properties [15-17]. Furthermore, their simpler synthesis, adjustable biological activity through ligand modification and ability to undergo redox and ligand-exchange reactions under physiological conditions have made metal complexes highly significant in medicinal chemistry [18].

Azomethine-based ligands coordinated with metal ions have been extensively investigated due to their remarkable selectivity and sensitivity [19]. In particular, hydrazide- and hydrazone-containing ligands possess significant structural flexibility, along with favourable electronic, magnetic, and chelating properties that facilitate metal complex formation [20,21]. These ligands can also exhibit keto-enol tautomerism, enabling the formation of complexes with unusual or higher coordination numbers [22,23]. Moreover, heteroatom containing cyclic ligands, especially those containing nitrogen and oxygen atoms, generally exhibit enhanced biological activity compared with purely carbon-based cyclic compounds. The presence of heteroatoms promotes intermolecular hydrogen bonding and strong interactions with enzymes and biological targets, thereby improving therapeutic potential [24,25].

Although numerous Schiff base metal complexes have been reported, studies on isoniazid-derived azomethine metal complexes remain limited despite their promising affinity toward biological targets. Recent reports have demonstrated that Schiff base metal complexes exhibit enhanced ligand-receptor interactions and significant therapeutic activity [26]. Therefore, in present study, novel Co(II), Ni(II), Cu(II), and Zn(II) complexes derived from an isoniazid-based Schiff base ligand were synthesised and characterised. Their biological activities including antidiabetic, anti-inflammatory and antioxidant properties, were evaluated. In addition, molecular docking studies were performed to investigate ligand-enzyme interactions, while DFT calculations were employed to understand the electronic properties and chemical reactivity of the ligand and its metal(II) complexes.

EXPERIMENTAL

All the solvents and reagents with analytical grade were procured from Sigma-Aldrich, USA. The progress of the reactions was monitored by the TLC plate. The TLC plate precoated with silica gel 60 F_{254} (0.2 mm thickness, Merck plate) and 60-120 mesh Merck silica gel used for column chromatography for purification, petroleum ether and ethyl acetate were used as the eluents. The ^{1}H and ^{13}C NMR analysis was performed on Bruker 500 MHz and 125 MHz instruments using DMSO-d_6 as a solvent. The ABSciex 5500+ Qtrap instrument was used for ESI-MS analysis. The Thermo Scientific Nicolet iS50 FT-IR spectrometer was used to measure the FT-IR spectra.

Synthesis of 2-(2-formylphenoxy)acetamide (2): Precursor (2-acetylsalicylic acid) (2 g, 0.011 mol) was dissolved in acetonitrile and in this solution, boc anhydride (2.55 mL, 0.011 mol) and $(NH_4)_2CO_3$ (3.51 g, 0.044 mol) were added followed by the addition of catalytic amount of pyridine and then finally the reaction mixture was stirred for 3 h. The completion of the reaction was monitored by TLC. After completing the reaction, the reaction mixture was diluted with ethyl acetate (150 mL), washed with water (150 mL) and brine solution (150 mL). The organic layer was separated and dried over anhydrous Na_2SO_4. Yield: 84%. Elemental anal. of $C_{15}H_{14}N_4O_3$: calcd. (found) %: C, 60.40 (60.41); H, 4.73 (4.71); N, 18.78 (18.75). ^{1}H NMR (500 MHz, DMSO-d_6, δ ppm): 10.50 (s, 1H, CH=O), 7.73 (br s, 1H, NH), 7.56 (br s, 1H, NH), 7.79 (d, 1H, Ar–H *ortho* to CH=O), 7.70 (d, 1H, Ar-H), 7.19-7.16 (m, 2H, Ar–H), 4.67 (s, 2H, CH_2–O); ^{13}C {^{1}H} NMR (126 MHz, DMSO-d_6): δ 190.7 (**C**H=O), 170.0 (**C**=ONH$_2$), 160.3 (**C**–O), 136.8 (**C**H–CH–C–O), 128.8 (**C**H–CCH=O), 125.0 (**C**–CH=O), 121.8 (**C**H–CH–C–CH=O), 114.0 (**C**H–C–O), 67.6 (**C**H$_2$).

Synthetic procedure for (*E*)-2-(2-((2-isonicotinoylhydrazono)methyl)phenoxy)acetamide (L): Intermediate **2** (3.0 g, 1.17 mmol) dissolved in ethanol (50 mL) was added to isoniazid (1.60 g, 1.17 mmol) solution was added in the presence of catalytic amount of acetic acid. The reaction mixture was refluxed for 3 h and the reaction was monitored by TLC. The reaction mixture was allowed to cool at room temperature and the white precipitate was filtered and dried over anhydrous Na_2SO_4 (**Scheme-I**). Yield: 83%; ^{1}H NMR (500 MHz, DMSO) δ 12.13 (s, 1H), 8.87 (s, 1H), 8.85 (d, 2H), 7.90-7.88 (m, 3H), 7.69 (s, 1H), 7.58 (s, 1H), 7.48 (bs, 1H), 7.13 (t, *J* = 7.5 Hz, 1H), 7.08 (d, *J* = 8.4 Hz, 1H), 4.62 (s, 2H). ^{13}C NMR (126 MHz, DMSO-) δ 170.15, 162.08., 156.84, 150.88, 146.15, 140.99, 132.31, 127.64, 122.70, 122.08, 121.88, 113.33,67.46.

Synthesis of metal(II) complexes: The ligand (**L**, 0.5 g, 0.133 mmol) was dissolved in warm methanol (20 mL), followed by the addition of the respective metal(II) salt solution (0.133 mmol in 5 mL methanol). The reaction mixture was stirred for 6 h at room temperature. The resulting metal(II) complexes were precipitated, filtered and washed with methanol. The metal(II) complexes were subsequently characterised and evaluated for biological studies. Yield: 80-85%.

Yield: 82%; elemental analysis of Cu(II) complex, $C_{15}H_{14}N_4O_3Cu$: calcd. (found) %: C, 49.79 (49.77); H, 3.90 (3.92); N, 15.48 (15.49); Cu, 17.56 (17.54).

Yield: 83%; elemental analysis of Co(II) complex, $C_{15}H_{14}N_4O_3Co$: calcd. (found) %: C, 50.43 (50.44); H, 3.95 (3.96); N, 15.68 (15.67); Co, 16.50 (16.49).

Yield: 81%; elemental analysis of Ni(II) complex, $C_{15}H_{14}N_4O_3Ni$: calcd. (found) %: C, 50.47 (50.46); H, 3.95 (3.96); N, 15.69 (15.68); Ni, 16.44 (16.42).

Yield: 82%; elemental analysis of Zn(II) complex, $C_{15}H_{14}N_4O_3Zn$: calcd. (found) %: C, 49.54 (49.55); H, 3.88 (3.89); N, 15.41 (15.42); Zn, 17.98 (17.97).

Biological studies

Antidiabetic activity: The antidiabetic activity of the metal(II) complexes was evaluated using the α-amylase inhibition assay and compared with a reference standard [27]. In brief, α-amylase enzyme solution (0.5 mg/mL) was incubated with the test complexes and standard in 20 mM sodium phosphate buffer (pH 6.9) at 25 ºC for 10 min. Subsequently, 1 mL of 1% starch solution was added and the reaction mixture was further incubated at 25 ºC for 30 min. The enzymatic reaction was terminated by the addition of 1 mL 3,5-dinitrosalicylic acid (DNSA) reagent, followed by heating in a water bath for 15 min. After cooling to room temperature, the absorbance was recorded at 540 nm using a UV-visible spectrophotometer. The percentage inhibition of α-amylase activity was calculated by comparing the absorbance of the treated samples with that of the control using following equation:

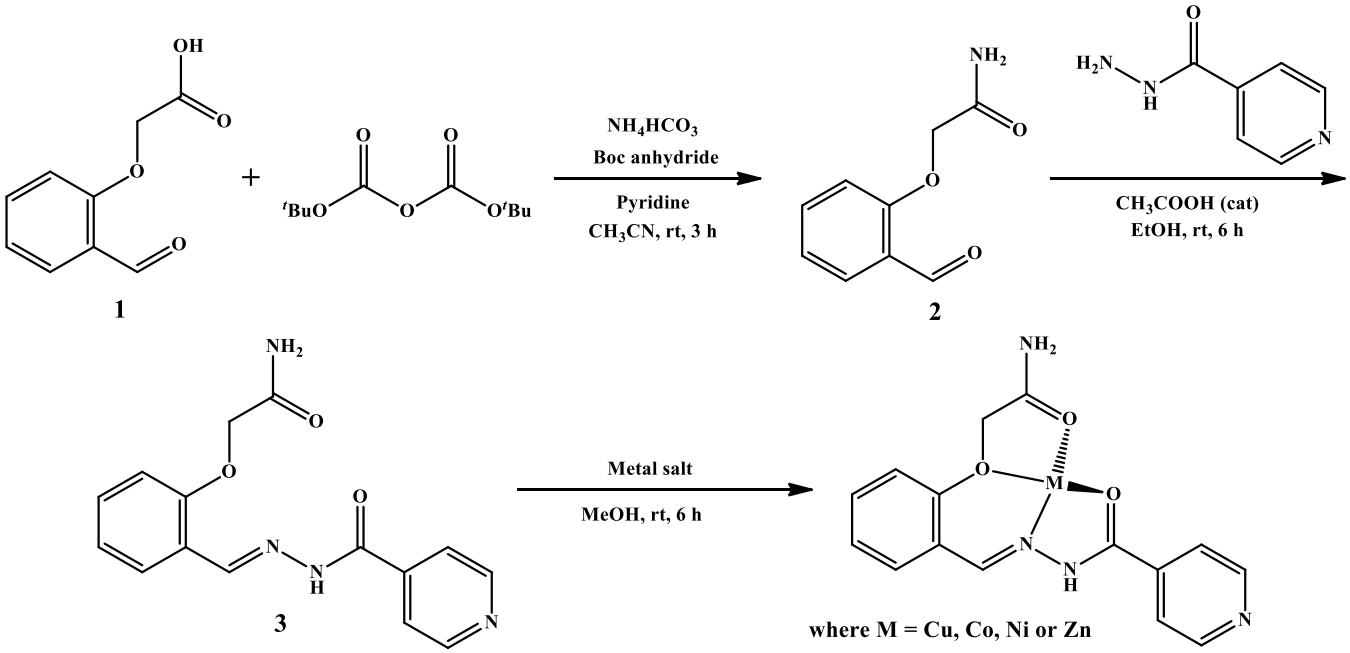

Scheme-I: Multi-layer synthesis of an isoniazid-based Schiff base metal complexes

$$\text{Inhibition (\%)} = \frac{A_t - A_c}{A_t} \times 100$$

where A_t: Absorbance of test; A_c: Absorbance of control.

Anti-inflammatory activity: The anti-inflammatory activity of the synthesised metal(II) complexes was evaluated using the bovine serum albumin (BSA) denaturation method, with diclofenac sodium used as the reference standard [28]. The metal(II) complexes and standard were dissolved in a minimal amount of DMF and diluted with phosphate buffer solution (0.2 M, pH 7.4), ensuring that the final DMF concentration did not exceed 2.5%. Subsequently, 1 mM BSA solution prepared in phosphate buffer was added to each sample and incubated at 37 ºC for 15 min. The reaction mixtures were then heated at 70 ºC for 30 min in a water bath to induce protein denaturation. After cooling to room temperature, the resulting turbidity was measured spectrophotometrically at 660 nm using a UV-visible spectrophotometer. The percentage inhibition of protein denaturation was calculated by comparing the absorbance values of the test samples with the control using following equation:

$$\text{Inhibition (\%)} = \frac{A_t - A_c}{A_t} \times 100$$

where A_t: absorbance of test; A_c: absorbance of control.

Antioxidant activity: The total antioxidant activity of ligand and its metal(II) complexes was evaluated using the phosphomolybdenum method [29]. An aliquot of reagent solution (3 mL) containing 0.6 M H_2SO_4, 28 mM Na_3PO_4, and 4 mM ammonium molybdate was added to different concentrations of the metal(II) complexes (25, 50, 100, 250 and 500 µg/mL). The reaction mixtures were incubated in a water bath at 95 ºC for 90 min to facilitate the reaction. After cooling to room temperature, the absorbance of the test samples and the standard (vitamin C) was measured at 695 nm using a UV-visible spectrophotometer. The total antioxidant activity was calculated using a standard equation.

$$\text{Total antioxidant activity} = \frac{A_t - A_c}{A_t} \times 100$$

Statistical analysis: Statistical analysis was carried out using Microsoft Excel 2019; Student's t-test was used for evaluating statistical significance between the treatments. A *p*-value of < 0.05 was considered statistically significant.

Molecular docking study: Molecular docking analysis was performed using the reported literature procedure [30]. Docking studies were carried out using Hex 8.0 software with the 1HNY crystal structure obtained from the Protein Data Bank (PDB, www.rcsb.org). The optimized three-dimensional structures of the metal complexes used for docking were generated from DFT calculations. Prior to docking, all co-crystallized ligands and water molecules were removed from the protein structure. Polar hydrogen atoms were added, while nonpolar hydrogen atoms were merged to prepare the protein for docking analysis.

Computational calculations: All computational studies were performed using Gaussian 09W software. Density functional theory (DFT) calculations were employed to determine the highest occupied molecular orbital (HOMO) and lowest unoccupied molecular orbital (LUMO) energies from the checkpoint files. The molecular geometries of the metal complexes were optimized using the B3LYP/LAN2DZ basis set [31]. The visualization of the optimized structures, HOMO-LUMO distributions and molecular electrostatic potential (MEP) surfaces was carried out using GaussView software.

RESULTS AND DISCUSSION

The synthesised Schiff base ligand and its metal(II) complexes were stable at room temperature and readily soluble in

DMF and DMSO solvents. Conductivity measurements indicated a 1:1 metal-to-ligand stoichiometric ratio. The low molar conductance (Λ_m) values of the ligand and its metal(II) complexes (6.8, 8.2, 7.1, 10.2, and 12.2 Ω^{-1} cm^2 mol^{-1} for ligand, Cu(II), Co(II), Ni(II) and Zn(II) complexes, respectively suggest their non-electrolytic nature.

NMR spectral studies: The ^{1}H NMR spectrum of intermediate **2** displayed signals corresponding to nine protons. The aldehyde proton appeared as a singlet at δ 10.50 ppm. Two broad singlets at δ 7.73 and 7.56 ppm were assigned to the amide NH_2 protons. Aromatic protons adjacent to the aldehyde and ether substituents resonated as doublets at δ 7.79 and 7.70 ppm, respectively, while the remaining aromatic protons appeared as a multiplet at δ 7.19-7.16 ppm (2H). The methylene protons adjacent to the ether oxygen and amide carbonyl group were observed as a singlet at δ 4.67 ppm (2H).

The ^{1}H NMR spectrum of the Schiff base ligand confirmed successful condensation with isoniazid. A characteristic singlet at δ 12.13 ppm was assigned to the hydrazide NH proton, while the azomethine proton (–CH=N–) appeared as a singlet at δ 8.87 ppm, confirming Schiff base formation. The pyridyl protons resonated at δ 8.85 and 7.90 ppm, whereas the carboxamide NH_2 protons appeared as broad singlets at δ 7.69 and 7.58 ppm. The methylene protons linked to the ether oxygen and carbonyl group appeared at δ 4.62 ppm, while the remaining aromatic protons were observed within the expected aromatic region.

The ^{13}C NMR spectrum of the ligand showed thirteen distinct carbon resonances for the fifteen-carbon system, indicating chemically non-equivalent carbon environments. The amide carbonyl carbon resonated at δ 170.1 ppm, while the amidic carbonyl carbon of the isoniazid moiety appeared at δ 162.1 ppm. The azomethine carbon (C=N) was observed at δ 146.2 ppm, confirming Schiff base formation. The aromatic carbon attached to the ether oxygen resonated at δ 156.8 ppm, and the methylene carbon linked to the ether oxygen and carbonyl group appeared at δ 67.5 ppm. The remaining aromatic carbons were observed in the expected region between δ 113.3 and 150.9 ppm, supporting the proposed ligand structure.

FT-IR studies: The structure of the ligand was further confirmed by FT-IR spectroscopy (Fig. 1). The FT-IR spectrum exhibited a characteristic band at 3362 cm^{-1} corresponding to the amide N–H stretching vibration. The aromatic C–H stretching vibration was observed around 3050 cm^{-1}, while the methylene (–CH_2–) stretching vibration appeared at 2954 cm^{-1}. Two distinct absorption bands at 1681 and 1648 cm^{-1} were assigned to the carbonyl stretching vibrations of the amide groups. The characteristic azomethine (C=N) stretching vibration was observed at 1538 cm^{-1}, confirming Schiff base formation. In addition, the ether (C–O) stretching vibration appeared at 1110 cm^{-1}. These characteristic absorption bands confirmed the presence of the expected functional groups and supported the proposed structure of the ligand.

The FT-IR spectra of the synthesized metal(II) complexes are shown in Fig. 2. All metal(II) complexes exhibited broad absorption bands around 3200 cm^{-1}, corresponding to aromatic and methylene C–H stretching vibrations. The amide N–H stretching vibrations were observed in the range of 3437-3363 cm^{-1}. Compared with the free ligand, clear shifts in the amide carbonyl and azomethine stretching frequencies were observed in the metal complexes. The azomethine stretching bands appeared in the range of 1550-1541 cm^{-1}, indicating coordination of the ligand to the metal ions through the azomethine nitrogen atom. The shifts in the carbonyl stretching frequencies further suggested the involvement of oxygen atoms from the ether and amide carbonyl groups in metal coordination. These spectral changes indicate strong metal–ligand interactions and redistribution of electron density within the ligand framework upon complex formation. The key characteristic FT-IR absorption bands of the ligand and its metal(II) complexes are summarized in Table-1.

Mass studies: The molecular weight of the ligand was confirmed by ESI-MS analysis in positive ion mode (Fig. 3a). The spectrum exhibited a molecular ion peak at *m/z* 298.8 corresponding to $[M+H]^+$ ion, confirming the formation of the

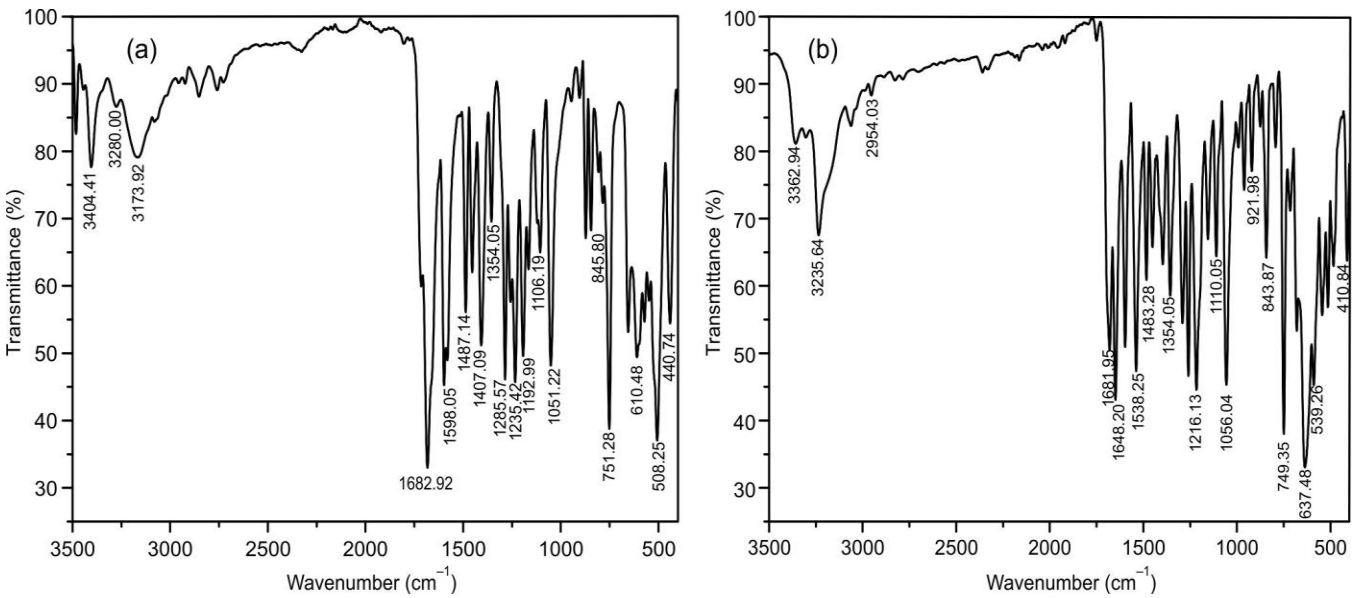

Fig. 1. FT-IR spectra of (a) intermediate 2 and (b) ligand

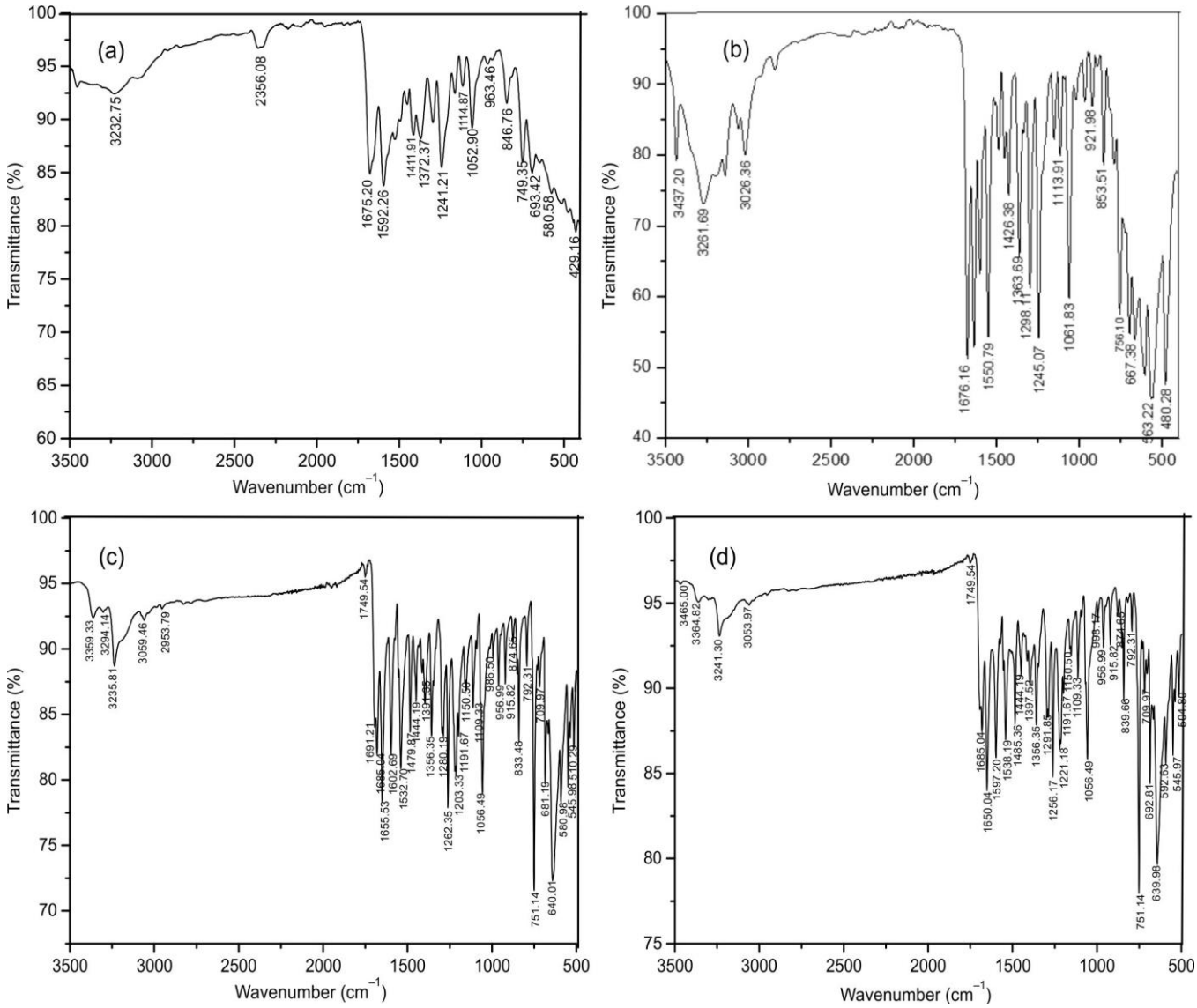

Fig. 2. FT-IR spectra of (a) Cu^{2+}, (b) Co^{2+}, (c) Ni^{2+} and (d) Zn^{2+} complexes

TABLE-1
CHARACTERISTICS KEY FT-IR (cm^{-1}) BANDS OF LIGAND AND ITS METAL(II) COMPLEXES

Functional group name	Ligand	Copper(II) complex	Cobalt(II) complex	Nickel(II) complex	Zinc(II) complex
Amide -NH-	3362	3434	3437	3359	3364
Aromatic	3235	3232	3261	3235	3241
Amide carbonyl	1681, 1648	1675	1676	1685, 1655	1685, 1650
Imine azomethine	1538	1592	1550	1532	1538

ligand. An additional peak observed at *m/z* 320.9 was assigned to the sodium adduct ion $[M+Na]^+$. ESI-MS analysis further supported the formation of the metal(II) complexes, showing molecular ion peaks corresponding to $[M+H]^+$ ions at *m/z* 360.7, 357.0, 356.8 and 362.7 for the Cu(II), Co(II), Ni(II), and Zn(II) complexes, respectively (Fig. 3b-e).

UV-visible spectroscopic studies: The electronic properties of the ligand and its metal(II) complexes were investigated by UV-visible spectroscopy. The free ligand exhibited two characteristic absorption bands at 305 and 328 nm, attributed to the π→π* transition of the azomethine group and the n→π* transition of the pyridyl aromatic system, respectively. Upon coordination with metal ions, clear spectral shifts were observed in the metal(II) complexes, where the π→π* transition bands shifted toward higher wavelengths by 4-12 nm, indicating strong metal-ligand interactions and increased conjugation within the coordinated system. The disappearance of the ligand n→π* transition band and the appearance of new absorption bands in the range of 364-382 nm were assigned to ligand-to-metal charge transfer (LMCT) transitions, confirming complex formation (Fig. 4). In addition, the Cu(II) complex exhibited a weak absorption band around 390 nm, characteristic of *d-d* electronic transition (Table-2).

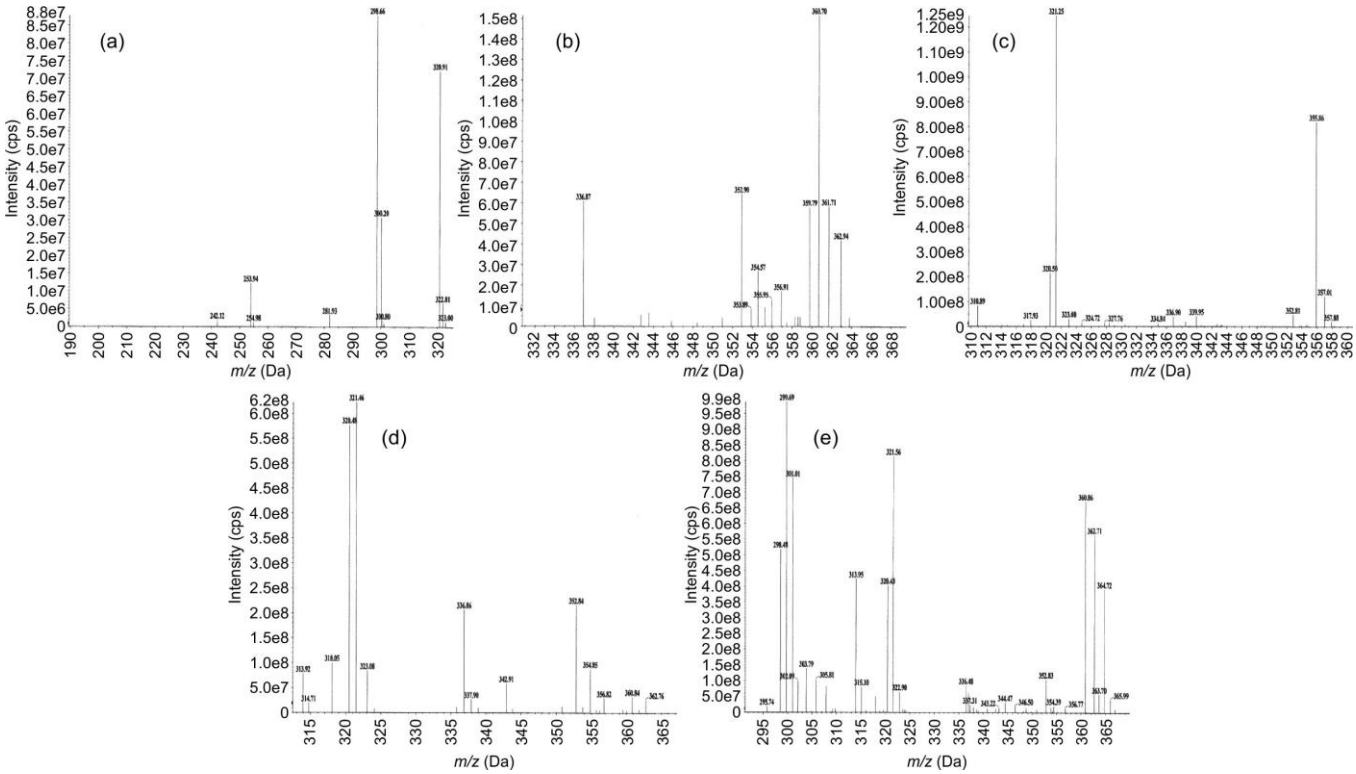

Fig. 3. Mass spectrum of (a) ligand, (b) Cu^{2+}, (c) Co^{2+}, (d) Ni^{2+} and (e) Zn^{2+} complexes

TABLE-2
UV-VISIBLE DATA (nm) OF LIGAND AND ITS METAL(II) COMPLEXES

Transitions	Ligand (Lig)	Copper(II) complex (CuC)	Cobalt(II) complex (CoC)	Nickel(II) complex (NiC)	Zinc(II) complex (ZnC)
π-π*	305	308	308	318	308
n-π*	328	–	332	328	336
LMCT	–	366	382	364	370

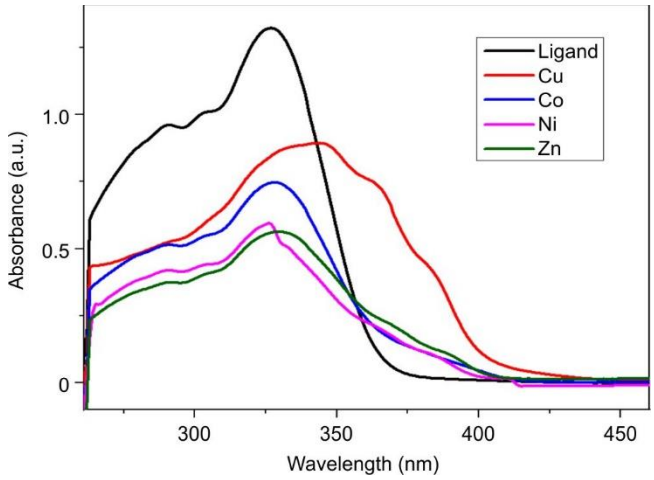

Fig. 4. Absorption spectra of the synthesised ligand and its metal(II) complexes

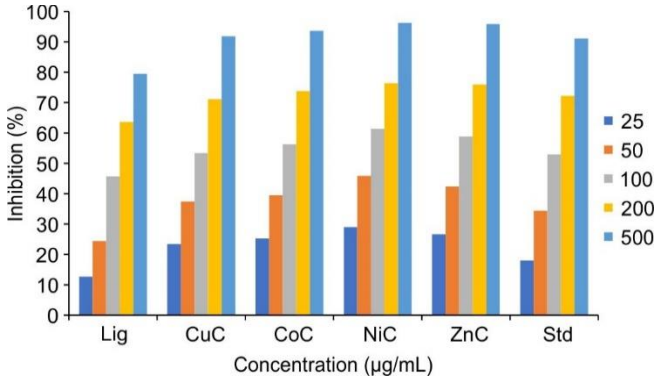

Fig. 5. *In vitro* antidiabetic activity of the ligand and its metal(II) complexes using α-amylase inhibition method. Statistical significance: $p < 0.05$

Biological studies

Antidiabetic activity: The antidiabetic activity of the synthesised ligand and its metal(II) complexes was evaluated using the α-amylase inhibition assay at different concentrations and compared with the reference standard (Fig. 5). All metal complexes exhibited significantly higher inhibitory activity than the free ligand and the standard drug. The free ligand showed 79.4% inhibition, whereas the Cu(II), Co(II), Zn(II) and Ni(II) complexes exhibited inhibition values of 91.8%, 93.6%, 95.8% and 96.2%, respectively. Among the investigated complexes, the Ni(II) complex demonstrated the highest antidiabetic activity, exceeding that of the standard drug (91.1%). The enhanced activity of the metal complexes may be attributed to improved interaction between the coordi-

nated metal centers and the enzyme active site. All experiments were performed in triplicate and the IC_{50} values for the ligand, Cu(II), Co(II), Ni(II), Zn(II), and standard were determined as 213.14, 132.98, 115.31, 79.4, 98.24 and 147.52 μg/mL, respectively.

Anti-inflammatory studies: The anti-inflammatory activity of the synthesised ligand and its metal(II) complexes was evaluated using the BSA denaturation assay and the results are presented in Fig. 6. All metal(II) complexes exhibited higher inhibition efficiency than the reference drug indicating significant anti-inflammatory potential. The standard drug showed 88.3% inhibition, while the free ligand exhibited 89.1% inhibition. Among the metal complexes, Cu(II), Co(II), Ni(II) and Zn(II) complexes demonstrated inhibition values of 91.1%, 93.7%, 96.6%, and 98.0%, respectively. The Zn(II) complex exhibited the highest anti-inflammatory activity, followed by the Ni(II) complex. The enhanced inhibition of BSA denaturation compared with α-amylase inhibition suggests stronger interaction of the complexes with inflammatory protein targets. All experiments were carried out in triplicate and the IC_{50} values for the ligand, Cu(II), Co(II), Ni(II), Zn(II) and standard were determined as 84.06, 65.46, 36.23, 47.33, 44.63, and 97.44 μg/mL, respectively. These findings indicate that the synthesised metal complexes possess promising anti-inflammatory properties.

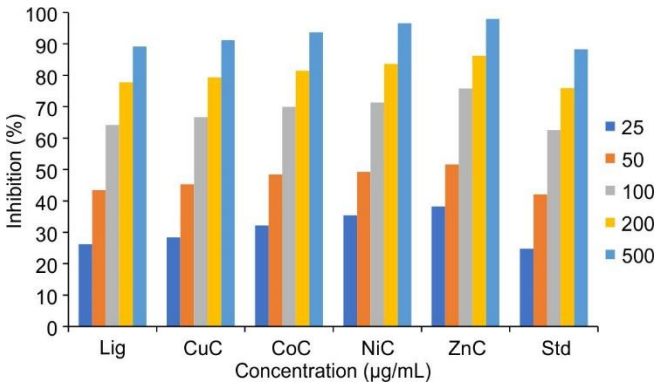

Fig. 6. *In vitro* anti-inflammatory activity of the ligand and its metal(II) complexes using BSA protein inhibition method. Statistical significance: $p < 0.05$

Total antioxidant activity: The antioxidant activity of the synthesised ligand and its metal(II) complexes was evaluated by the phosphomolybdenum assay and the results are shown in Fig. 7. Although the antioxidant activities of the ligand and its complexes were lower than that of the standard ascorbic acid (99.4% inhibition), the synthesized metal(II) complexes exhibited significantly enhanced activity compared with the free ligand and previously reported metal complexes [32]. The

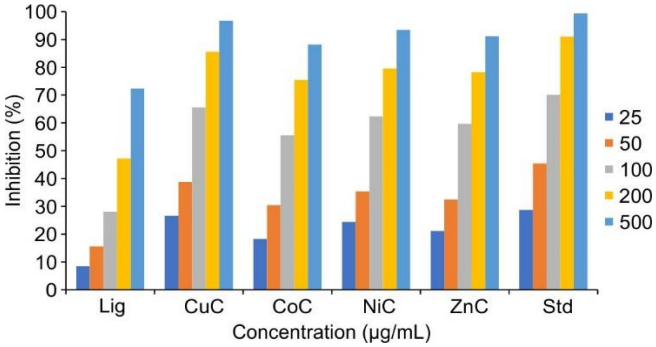

Fig. 7. Total content of antioxidant studies of the ligand and its metal(II) complexes in an *in vitro* manner. Statistical significance: $p < 0.05$

free ligand showed the lowest antioxidant activity with 72.3% inhibition. Among the metal(II) complexes, Co(II), Zn(II) and Ni(II) complexes exhibited inhibition values of 88.21%, 91.1% and 93.4%, respectively, while the Cu(II) complex demonstrated the highest antioxidant activity with 96.7% inhibition. The improved antioxidant performance of the synthesized metal(II) complexes may be attributed to enhanced electron transfer and radical scavenging ability upon metal coordination. All experiments were performed in triplicate and the IC_{50} values for the ligand, Cu(II), Co(II), Ni(II), Zn(II) and standard were determined as 296.35, 79.44, 148.02, 105.96, 125.73, and 43.62 μg/mL, respectively.

Molecular docking studies: Molecular docking analysis was performed to investigate the binding affinity and interaction behaviour of the synthesised metal(II) complexes toward the target protein (1HNY) [33-37]. The optimized ligand structures were docked into the active site of the protein to identify the most stable binding conformations and evaluate their interaction energies, hydrogen bonding and binding stability. The docking results including hydrogen-bond interactions and binding energies are summarized in Table-3, while the three-dimensional binding interactions are illustrated in Fig. 8.

Among the investigated complexes, the Zn(II) complex exhibited the strongest binding affinity with a binding energy of -271.76 kJ/mol. The complex formed three hydrogen-bond interactions with amino acid residues HIS299, TRP59, and ASP300, involving both conventional and carbon–hydrogen bonding interactions. The Cu(II) complex formed two hydrogen bonds with LEU211 and ASN250, showing a binding energy of -263.04 kJ/mol. Similarly, the Co(II) complex interacted with LEU211 and SER3 through two hydrogen bonds and exhibited a binding energy of -250.38 kJ/mol. The Ni(II) complex formed a single hydrogen bond with ASP197 and showed a binding energy of -259.75 kJ/mol. Based on the docking energies, the interaction strength of the complexes followed the order: Zn > Cu > Ni > Co. These results demons-

TABLE-3
INTERACTION OF METAL COMPLEX WITH α-AMYLASE ENZYME (1HNY.pdb)

Metal complex	Binding energy (kJ/mol)	No. of hydrogen bonding	Interacted amino acid residues and their bond length
CuC	-263.04	2	LEU211[a] (2.56 Å), ASN250[a] (3.32 Å)
CoC	-250.38	2	LEU211[a] (2.89 Å), SER3[a] (3.04 Å)
NiC	-259.75	1	ASP197[b] (2.79 Å)
ZnC	-271.76	3	ASP300[b] (2.95 Å), HIS299[a,b] (1.59 Å), TRP59[b] (2.11 Å)

[a]Conventional hydrogen bonding interaction, [b]Carbon hydrogen bonding interaction.

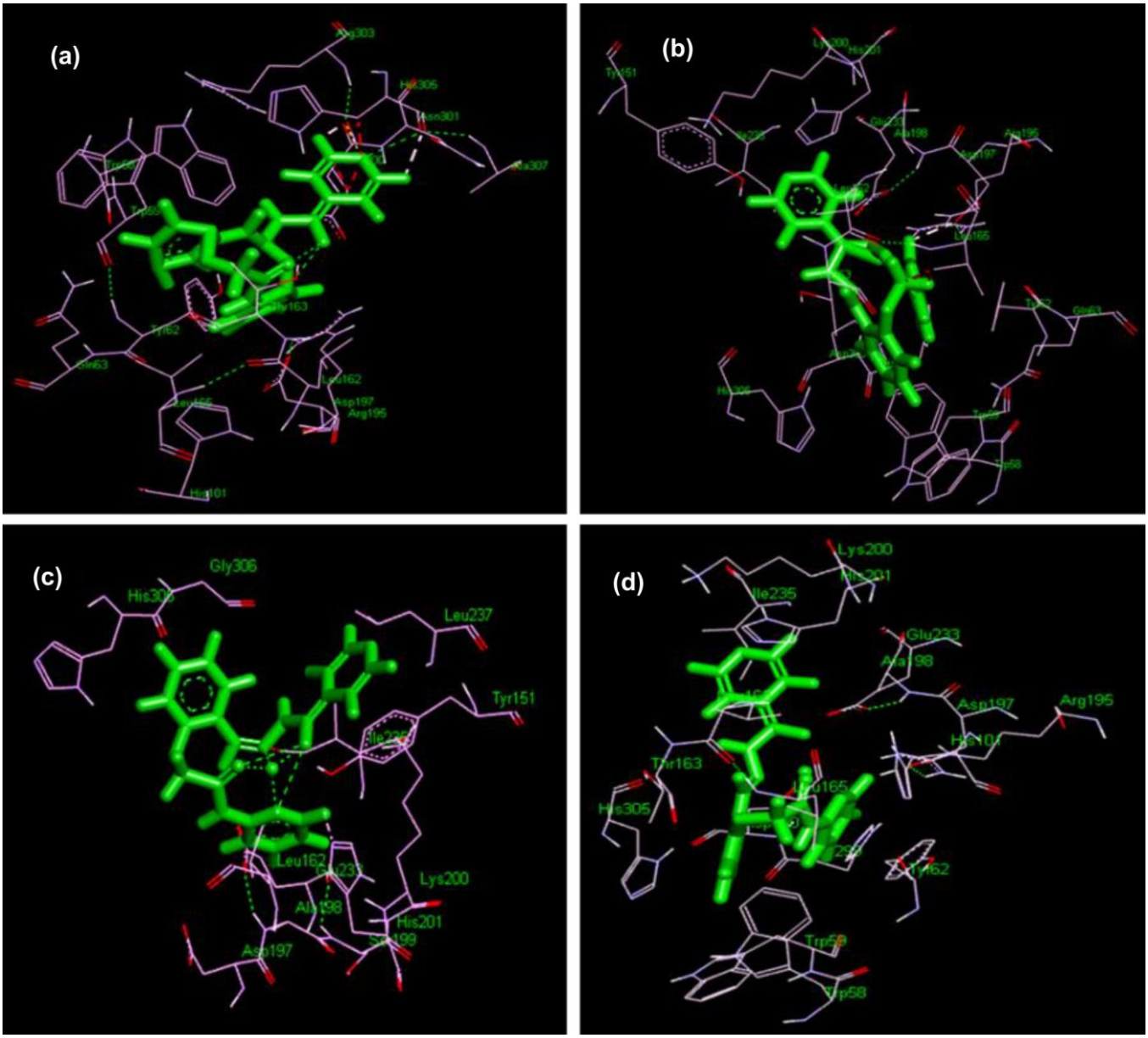

Fig. 8. Molecular docking studies of the synthesised metal(II) complexes (a) Cu^{2+}, (b) Co^{2+}, (c) Ni^{2+} and (d) Zn^{2+}

trate strong interactions between the metal(II) complexes and the active site residues of the 1HNY protein, supporting their promising biological activity.

DFT studies: Density functional theory (DFT) calculations were performed to investigate the electronic properties, molecular stability and chemical reactivity of the synthesised metal(II) complexes [38-44]. The optimized frontier molecular orbitals (HOMO and LUMO) provided valuable information regarding electron distribution, charge transfer behaviour and ligand–metal interactions (Fig. 9). The Co(II) complex exhibited the largest HOMO–LUMO energy gap indicating higher stability, greater chemical hardness, and comparatively lower interaction with biomolecules. In contrast, the Zn(II) complex showed the smallest band gap and highest global softness, suggesting enhanced electron transfer ability, higher chemical reactivity and stronger interaction with biological targets, which correlates well with its superior biological activity observed experimentally. The Ni(II) complex displayed electronic properties similar to those of the Zn(II) complex, while the Cu(II) complex exhibited intermediate behaviour with moderate band gap and reactivity. The HOMO electron density of the Co(II) complex was mainly distributed over the amine region, whereas in the Cu(II) complex, electron density was localized over the pyridyl moiety and shifted toward the metal center in the LUMO state, indicating ligand-to-metal charge transfer characteristics. The calculated band gap, global hardness, softness, chemical potential and electrophilicity index values demonstrated that lower band gap and higher softness favour stronger biomolecular interactions and enhanced biological activity (Table-4). Thus, based on the DFT results are consistent with the molecular docking and *in vitro* biological studies confirming that the Zn(II) complex possesses the highest reactivity and biological potential among the synthesised metal(II) complexes.

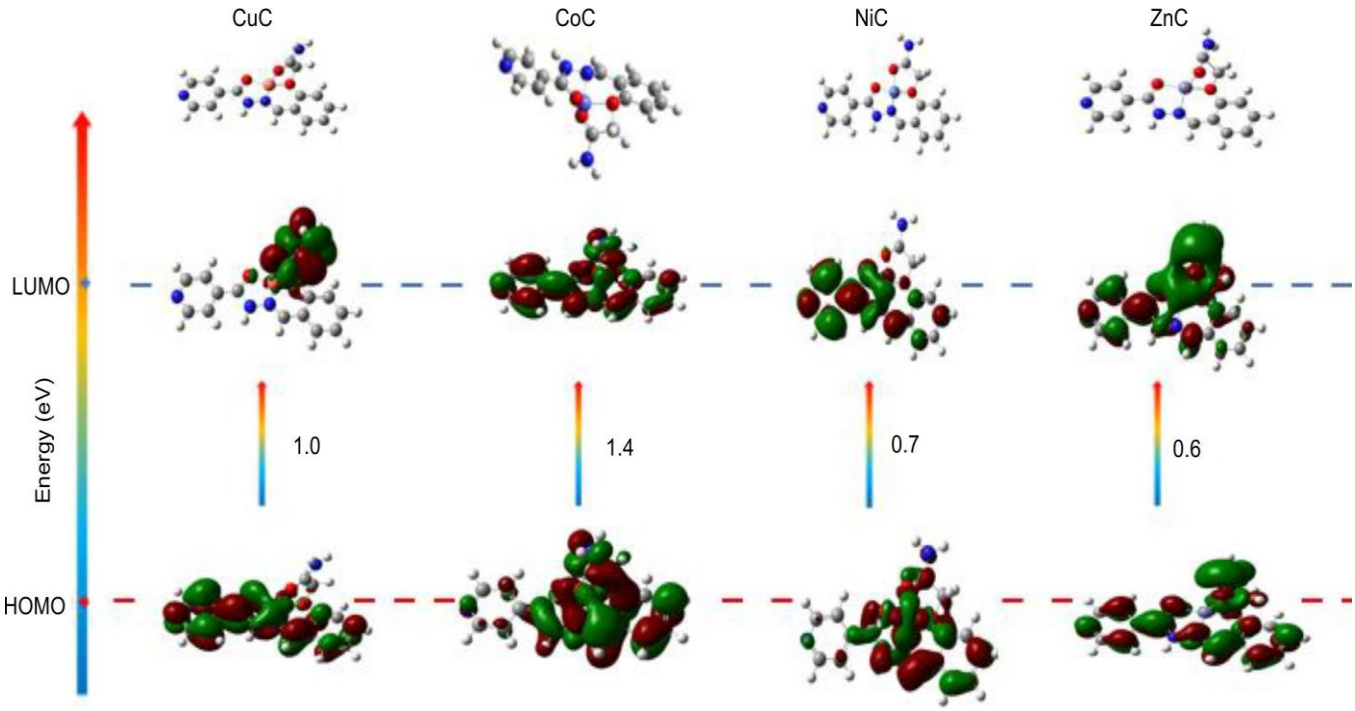

Fig. 9. Frontier molecular analysis of synthesised complexes (a) Cu^{2+}, (b) Co^{2+}, (c) Ni^{2+} and (d) Zn^{2+}

TABLE-4
DATA OBTAINED FROM THE DFT STUDIES

Compound	HOMO (eV)	LUMO (eV)	Band gap (ΔE) (eV)	Chemical potential (eV)	Global hardness (eV)	Global softness (eV^{-1})	Electrophilicity index (eV)
CuC	-2.5285	-1.4661	1.0623	-1.9973	0.5311	0.9413	3.7552
CoC	-2.4504	-1.0386	1.441	-1.7445	0.7058	0.7083	2.1558
NiC	-2.5375	-1.7943	0.743	-2.1659	0.3715	1.3456	6.3126
ZnC	-3.0003	-2.3388	0.661	-2.6696	0.3307	1.5116	10.7735

Molecular electrostatic potential (MEP): Molecular electrostatic potential (MEP) analysis was performed to investigate the electron density distribution and potential reactive sites of the synthesised metal(II) complexes (Fig. 10) [45,46]. The MEP surfaces were generated from the optimized geometries obtained through DFT calculations. In the MEP maps, red regions represent areas of high electron density and negative electrostatic potential, indicating favourable sites for electrophilic attack and hydrogen-bond acceptor interactions, whereas blue regions correspond to positive electrostatic potential and potential nucleophilic interaction sites. Green regions indicate electronically neutral surfaces.

The MEP profiles revealed that the oxygen atoms in all complexes predominantly appeared in red regions, confirming their electron-rich nature and involvement in intermolecular interactions. In contrast, the Co(II) complex displayed more pronounced blue regions around the metal center, suggesting a relatively higher positive charge density and Lewis acidic character. The pyridyl nitrogen atoms also exhibited electron-rich regions due to the presence of lone-pair electrons, which may facilitate hydrogen-bond interactions with biological targets. The aromatic hydrogen atoms mainly appeared in green regions indicating neutral character; however, they may contribute to stabilizing biomolecular interactions through π-π stacking and electrostatic interactions.

Conclusion

A series of novel isoniazid-derived Schiff base metal(II) complexes of Co(II), Ni(II), Cu(II) and Zn(II) were successfully synthesized and characterized using elemental, spectroscopic and conductivity analyses. The results confirmed coordination of the ligand through azomethine nitrogen and oxygen donor atoms, forming stable non-electrolytic complexes with 1:1 metal-to-ligand stoichiometry. Biological studies demonstrated that metal coordination significantly enhanced the antidiabetic, anti-inflammatory and antioxidant activities compared with the free ligand. Among the synthesized complexes, the Zn(II) and Ni(II) complexes exhibited superior antidiabetic and anti-inflammatory activities, while the Cu(II) complex showed the highest antioxidant activity. The enhanced biological performance is attributed to improved electron delocalisation and stronger interaction of the metal complexes with biological targets. Molecular docking studies revealed strong binding interactions between the metal(II) complexes and the 1HNY protein, with the Zn(II) complex showing the highest binding affinity. DFT calculations further supported the experimental findings by correlating lower HOMO-LUMO energy gaps and higher global softness with enhanced biological activity. MEP analysis identified the oxygen and nitrogen atoms as the major reactive sites involved in biomolecular interactions.

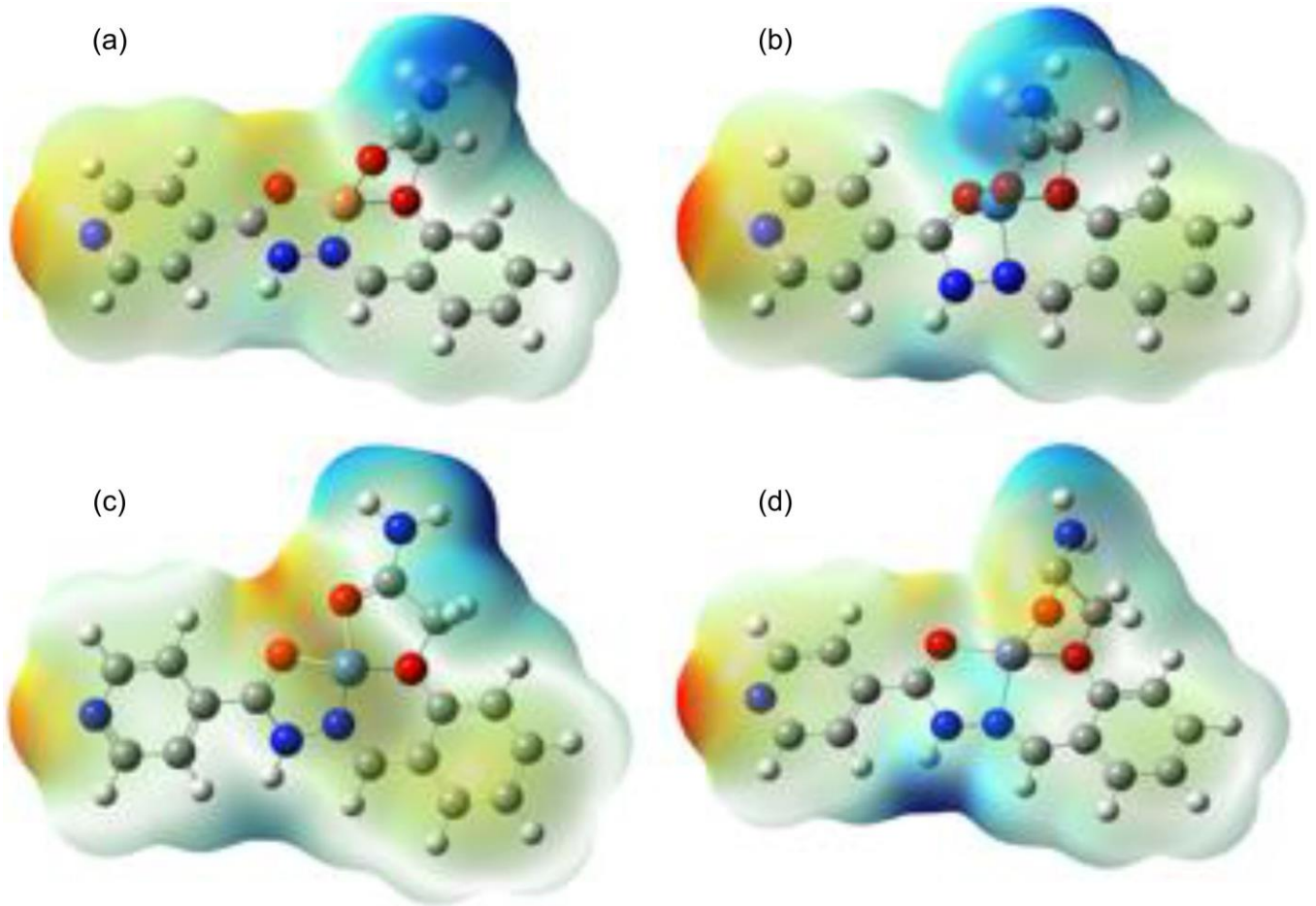

Fig. 10. Molecular electrostatic mapping of (a) Cu^{2+}, (b) Co^{2+}, (c) Ni^{2+} and (d) Zn^{2+} complexes

CONFLICT OF INTEREST

The authors declare that there is no conflict of interests regarding the publication of this article.

DECLARATION OF AI-ASSISTED TECHNOLOGIES

During the preparation of this manuscript, the authors used an AI-assisted tool(s) to improve the language. The authors reviewed and edited the content and take full responsibility for the published work.

REFERENCES

1. H. Beck, M. Härter, B. Ha, C. Schmeck and L. Baerfack, *Drug Discov. Today*, **27**, 1560 (2022); https://doi.org/10.1016/j.drudis.2022.02.015
2. C.M. da Silva, D.L. da Silva, L.V. Modolo, R.B. Alves, M.A. de Resende, C.V.B. Martins and Â. de Fátima, *J. Adv. Res.*, **2**, 1 (2011); https://doi.org/10.1016/j.jare.2010.05.004
3. Y. Mohini, R.B.N. Prasad, M.S.L. Karuna, C.G. Kumar, M. Poornima and P. Sujitha, *Med. Chem. Res.*, **22**, 4360 (2013); https://doi.org/10.1007/s00044-012-0450-y
4. M. Krátký, K. Konečná, O. Janďourek, A. Diepoltová, P. Vávrová, B. Voxová, M. Vejsová, P. Bárta, and S. Bősze, *Microbiol. Spectr.*, **11**, e03064-22 (2023); https://doi.org/10.1128/spectrum.03064-22
5. L.X. Cheng, J.J. Tang, H. Luo, X.J. Jin, F. Dai, Y. Yang, Y.P. Qian, X.-Z. Li and B. Zhou, *Bioorg. Med. Chem. Lett.*, **20**, 2417 (2010); https://doi.org/10.1016/j.bmcl.2010.03.039
6. S. Nidhi, Siddharam, D.P. Rao, A.K. Gautam, A. Verma and Y. Gautam, *Results Chem.*, **13**, 101941 (2025); https://doi.org/10.1016/j.rechem.2024.101941
7. P.M. Thakor, J.D. Patel, R.J. Patel, S.H. Chaki, A.J. Khimani, Y.H. Vaidya, A.P. Chauhan, A.B. Dholakia, V.C. Patel, A.J. Patel, N.H. Bhavsar and H.V. Patel,, *ACS Omega*, **9**, 35431 (2024); https://doi.org/10.1021/acsomega.4c02007
8. R. Kumar, A.A. Singh, U. Kumar, P. Jain, A.K. Sharma, C. Kant and M.S. Haque Faizi, *J. Mol. Struct.*, **1294**, 136346 (2023); https://doi.org/10.1016/j.molstruc.2023.136346
9. S. Rollas, N. Gulerman and H. Erdeniz, *Farmaco*, **57**, 171 (2002); https://doi.org/10.1016/S0014-827X(01)01192-2
10. H. Bayrak, A. Demirbas, N. Demirbas and S.A. Karaoglu, *Eur. J. Med. Chem.*, **44**, 4362 (2009); https://doi.org/10.1016/j.ejmech.2009.05.022
11. V.U. Kamble, A.S. Patil and S.P. Badami, *J. Incl. Phenom. Macrocycl. Chem.*, **68**, 347 (2010); https://doi.org/10.1007/s10847-010-9794-4
12. J. Ceramella, D. Iacopetta, A. Catalano, F. Cirillo, R. Lappano and M.S. Sinicropi, *Antibiotics*, **11**, 191 (2022); https://doi.org/10.3390/antibiotics11020191
13. E. Pauwels, V. Stoven and Y. Yamanishi, *BMC Bioinformatics*, **12**, 169 (2011); https://doi.org/10.1186/1471-2105-12-169
14. M.S.A. Hazer, S. Malola and H. Häkkinen, *Phys. Chem. Chem. Phys.*, **26**, 21954 (2024); https://doi.org/10.1039/D4CP00848K
15. T. Guchhait, M. Giri and S.P. Mishra, *J. Coord. Chem.*, **77**, 49 (2024); https://doi.org/10.1080/00958972.2024.2304156
16. K.N. Aziz, K.M. Ahmed, R.A. Omer, A.F. Qader and E.I. Abdulkareem, *Rev. Inorg. Chem.*, **45**, 1 (2025); https://doi.org/10.1515/revic-2024-0035

17. A.D. Garnovskii, A.P. Sadimenko, M.I. Sadimenko and D.A. Garnovskii, *Coord. Chem. Rev.*, **173**, 31 (1998); https://doi.org/10.1016/S0010-8545(98)00084-8
18. C.-H. Leung, S. Lin, H.-J. Zhong and D.-L. Ma, *Chem. Sci.*, **6**, 871 (2015); https://doi.org/10.1039/C4SC03094J
19. C. Imrie, P. Engelbrecht, C. Loubser and C.W. McCleland, *Appl. Organomet. Chem.*, **15**, 1 (2001); https://doi.org/10.1002/1099-0739(200101)15:1<1::AID-AOC109>3.0.CO; 2-3
20. Y. Li, J. Sui, L.-S. Cui and H.-L. Jiang, *J. Am. Chem. Soc.*, **145**, 1359 (2023); https://doi.org/10.1021/jacs.2c11926
21. S. Anand, A. Muthusamy and S. Dineshkumar, *J. Mol. Struct.*, **1248**, 131502 (2022); https://doi.org/10.1016/j.molstruc.2021.131502
22. U. Kendur, G.H. Chimmalagi, S.M. Patil, K.B. Gudasi and C.S. Frampton, *Appl. Organomet. Chem.*, **32**, e4278 (2018); https://doi.org/10.1002/aoc.4278
23. A. Bargan, M.F. Zaltariov, A. Vlad, A.-M.-C. Dumitriu, A. Soroceanu, A.-M. Macsim, M. Dascalu, C.D. Varganici, M. Cazacu and S. Shova, *Arab. J. Chem.*, **13**, 3100 (2020); https://doi.org/10.1016/j.arabjc.2018.09.001
24. N. Kerru, L. Gummidi, S. Maddila, K.K. Gangu and S.B. Jonnalagadda, *Molecules*, **25**, 1909 (2020); https://doi.org/10.3390/molecules25081909
25. S. Horowitz and R.C. Trievel, *J. Biol. Chem.*, **287**, 41576 (2012); https://doi.org/10.1074/jbc.R112.418574
26. D.A. Jeniva, K. Geetha, R. Sribalan, S. Praveen, R. Prabakarakrishnan and S. Rajamanickam, *J. Mol. Struct.*, **1358**, 145266 (2026); https://doi.org/10.1016/j.molstruc.2026.145266
27. R. Sankar and T.M. Sharmila, *Bioorg. Chem.*, **154**, 108010 (2025); https://doi.org/10.1016/j.bioorg.2024.108010
28. S. Umapathy, P. Govindaraj and R. Krishnan, *J. Coord. Chem.*, **70**, 3213 (2017); https://doi.org/10.1080/00958972.2017.1362674
29. R. Sankar and T.M. Sharmila, *Bioorg. Chem.*, **154**, 108010 (2025); https://doi.org/10.1016/j.bioorg.2024.108010
30. S. Geetha, R. Sribalan and S. Lakshmi, *Chemical Physics Impact*, **8**, 100608 (2024); https://doi.org/10.1016/j.chphi.2024.100608
31. M.J. Frisch, G.W. Trucks, H.B. Schlegel, G.E. Scuseria, M.A. Robb, J.R. Cheeseman, G. Scalmani, V. Barone, B. Mennucci, G.A. Petersson, H. Nakatsuji, M. Caricato, X. Li, H.P. Hratchian, A.F. Izmaylov, J. Bloino, G. Zheng, J.L. Sonnenberg, M. Hada, M. Ehara, K. Toyota, R. Fukuda, J. Hasegawa, M. Ishida, T. Nakajima, Y. Honda, O. Kitao, H. Nakai, T. Vreven, J.A. Montgomery Jr., J.E. Peralta, F. Ogliaro, M. Bearpark, J.J. Heyd, E.N. Brothers, K.N. Kudin, V.N. Staroverov, R. Kobayashi, J. Normand, K. Raghavachari, A. Rendell, J.C. Burant, S.S. Iyengar, J. Tomasi, M. Cossi, N. Rega, J. M. Millam, M. Klene, J.E. Knox, J.B. Cross, V. Bakken, C. Adamo, J. Jaramillo, R. Gomperts, R. E. Stratmann, O. Yazyev, A.J. Austin, R. Cammi, C. Pomelli, J.W. Ochterski, R.L. Martin, K. Morokuma, V.G. Zakrzewski, G.A. Voth, P. Salvador, J.J. Dannenberg, S. Dapprich, A.D. Daniels, Ö. Farkas, J.B. Foresman, J.V. Ortiz, J. Cioslowski and D.J. Fox, Gaussian 09, Revision D.01, Gaussian, Inc., Wallingford, CT, USA (2009).
32. G. Pizzino, N. Irrera, M. Cucinotta, G. Pallio, F. Mannino, V. Arcoraci, F. Squadrito, D. Altavilla and A. Bitto, *Oxid. Med. Cell. Longev.*, **2017**, 8416763 (2017); https://doi.org/10.1155/2017/8416763
33. A.M. Dar and S. Mir, *J. Anal. Bioanal. Technol.*, **8**, 356 (2017); https://doi.org/10.4172/2155-9872.1000356
34. R. Rohs, I. Bloch, H. Sklenar and Z. Shakked, *Nucleic Acids Res.*, **33**, 7048 (2005); https://doi.org/10.1093/nar/gki1008
35. I.A. Guedes, C.S. de Magalhães and L.E. Dardenne, *Biophys. Rev.*, **6**, 75 (2014); https://doi.org/10.1007/s12551-013-0130-2
36. S. Agarwal, D. Chadha and R. Mehrotra, *J. Biomol. Struct. Dyn.*, **33**, 1653 (2015); https://doi.org/10.1080/07391102.2014.968874
37. D. Seeliger and B.L. de Groot, *J. Comput. Aided Mol. Des.*, **24**, 417 (2010); https://doi.org/10.1007/s10822-010-9352-6
38. D.S. Sholl and J.A. Steckel, Density Functional Theory: A Practical Introduction, Wiley (2009)
39. T.V. Mourik, M. Bühl and M.-P. Gaigeot, *Phil. Trans. R. Soc. A*, **372**, 20120488 (2014); https://doi.org/10.1098/rsta.2012.0488
40. A.S. Murugan, M. Kiruthika, E.R.A. Noelson, P. Yogapandi and J. Annaraj, *Arab. J. Chem.*, **14**, 102910 (2021); https://doi.org/10.1016/j.arabjc.2020.11.016
41. S. Kumar, S.M. Arumugam, S. Sharma, S. Mahala, B. Devi and S. Elumalai, *J. Mol. Catal.*, **533**, 112757 (2022).
42. P. Makkar and N.N. Ghosh, *RSC Adv.*, **11**, 27897 (2021); https://doi.org/10.1039/D1RA04876G
43. M. Raftani, T. Abram, A. Azaid, R. Kacimi, M.N. Bennani and M. Bouachrine, *Mater. Today Proc.*, **45**, 7334 (2021); https://doi.org/10.1016/j.matpr.2020.12.1228
44. M. Bharathi, S. Shreedevi and R. Sribalan, *J. Mol. Struct.*, **1308**, 138060 (2024); https://doi.org/10.1016/j.molstruc.2024.138060
45. S. Lakshminarayanan, V. Jeyasingh, K. Murugesan, N. Selvapalam and G. Dass, *J. Photochem. Photobiol.*, **6**, 100022 (2021); https://doi.org/10.1016/j.jpap.2021.100022
46. H. Weinstein, R. Osman, J.P. Green and S. Topiol, in eds.: P. Politzer and D.G. Truhlar, Electrostatic Potentials as Descriptors of Molecular Reactivity: The Basis for Some Successful Predictions of Biological Activity, In: Chemical Applications of Atomic and Molecular Electrostatic Potentials, Eds. Boston, MA, USA: Springer (1981); https://doi.org/10.1007/978-1-4757-9634-6_14